INSTITUTE OF PHYSICS PUBLISHING NANOTECHNOLOGY
Nanotechnology **16** (2005) S522–S530 doi:10.1088/0957-4484/16/7/029

Diffusion of water and sodium counter-ions in nanopores of a β-lactoglobulin crystal: a molecular dynamics study

Kourosh Malek[1], **Theo Odijk**[2] **and Marc-Olivier Coppens**[1]

[1] Physical Chemistry and Molecular Thermodynamics, DelftChemTech, Faculty of Applied Sciences, Delft University of Technology, Julianalaan 136, 2628 BL Delft, The Netherlands
[2] Theory of Complex Fluids, Kluyver Laboratory for Biotechnology, Faculty of Applied Sciences, Delft University of Technology, PO Box 5057, 2600 GB Delft, The Netherlands

Received 19 January 2005, in final form 10 May 2005
Published 2 June 2005
Online at stacks.iop.org/Nano/16/S522

Abstract
The dynamics of water and sodium counter-ions (Na^+) in a $C222_1$ orthorhombic β-lactoglobulin crystal is investigated by means of 5 ns molecular dynamics simulations. The effect of the fluctuation of the protein atoms on the motion of water and sodium ions is studied by comparing simulations in a rigid and in a flexible lattice. The electrostatic interactions of sodium ions with the positively charged LYS residues inside the crystal channels significantly influence the ionic motion. According to our results, water molecules close to the protein surface undergo an anomalous diffusive motion. On the other hand, the motion of water molecules further away from the protein surface is normal diffusive. Protein fluctuations affect the diffusion constant of water, which increases from 0.646 ± 0.108 to 0.887 ± 0.41 nm^2 ns^{-1}, when protein fluctuations are taken into account. The pore size (0.63–1.05 nm) and the water diffusivities are in good agreement with previous experimental results. The dynamics of sodium ions is disordered. LYS residues inside the pore are the main obstacles to the motion of sodium ions. However, the simulation time is still too short for providing a precise description of anomalous diffusion of sodium ions. The results are not only of interest for studying ion and water transport through biological nanopores, but may also elucidate water–protein and ion–protein interactions in protein crystals.

1. Introduction

Understanding the behaviour of solvent and ions near dissolved proteins is of great importance in revealing protein structure and functionality [1–5]. Dynamic properties (e.g., mobility and structural organization) of water and counter-ions at the protein–water interface differ from those in the bulk [2, 5]. When proteins make up the lining of small pores, water and ions affect the passage of substances through such pores [5, 6]. With this prospect, the pore structure of a protein crystal offers a useful test system for investigating dynamics of water and ion motion in a confined biological region [6–8]. Protein crystals contain biological nanopores that range in width from approximately 0.3 nm up to 10 nm, and occupy 25–75% of the crystal volume. Their porosity is comparable to that of inorganic porous catalysts and sorbents such as zeolites and silica gel [7]. Cross-linked protein crystals have recently been proposed for chemical and pharmaceutical applications as extremely stable catalysts [7, 8] and as selective (chiral) separation media [9]. Properties of intracrystalline water molecules and ions, and their transport through the crystal, are essential to these applications.

The ability of small solutes to enter and leave protein crystals has been known for a long time. This property

was initially used in preparation of isomorphous derivatives in protein crystallography [6, 10]. Several studies have focused on the experimental determination of the solute and water transport in protein crystals [11–14]. Some reliable experimentally based diffusion models have been proposed recently [15]. However, there have been few attempts in the direction of theoretical or computational studies of diffusion in protein crystals. Recently, we carried out dynamic Monte Carlo and Brownian dynamics simulations, to study electrostatic and steric confinement effects on the mobility of small spherical probes in lysozyme crystals [16]. Molecular dynamics (MD) simulations provide a more detailed way to study protein crystals, because they allow accounting for the fluctuation of protein atoms, and the structure of the diffusing molecules and ions. MD simulations have recently been used to study the structure related properties of protein crystals [17–20].

One of the first attempts to measure diffusion in protein crystals was by Bishop and Richards [6], who studied diffusion of a series of bromine-containing solutes into single, cross-linked crystals of β-lactoglobulin (βLG). This protein has been widely studied since it was first purified from cow's milk in 1934 [21]. βLG is a globular, acid-stable protein containing 152 residues. It constitutes approximately two-thirds of the whey fraction of ruminant milk [22]. Interestingly, βLG has a markedly high α-helical propensity [23, 24]. Thus, it might serve as a suitable model for studying the effect of protein fluctuations on the dynamics of water and (sodium) counter-ion motion through the pores in protein crystals. To our knowledge, there have been no prior MD studies on fluctuations and correlations in crystalline βLG. Moreover, immobilized βLG has recently been used as a chiral stationary phase in high performance liquid chromatography [25]. Understanding the nature of transport of small molecules and ions through βLG crystals is essential in practical applications of this protein crystal either as a porous separation medium or as a (bio)catalyst [7, 16]. Because of the similarities between channels in protein crystals and in biological membranes, and the much greater precision with which the atomic structure and properties of many protein crystals are known from x-ray studies, protein crystals serve as a suitable model for studying diffusion of ions and small molecules in biological channels, and simulations for protein crystals provide new insights into diffusion in biological channels in a general sense as well [11, 14, 26]. Both the water–βLG and ion–βLG interactions were studied experimentally [27, 28]. Several fundamental issues remained unanswered, such as those of the detailed nature of the diffusive motion of water molecules and ions, and the effect of protein fluctuations on water and ion motions inside the pores of the protein crystals. We wish to answer those questions by means of all-atom MD simulations.

2. Model and methodology

2.1. Protein crystal model

We used MD simulations to examine water and ion motions over a period of 5 ns in a ($C222_1$) βLG orthorhombic lattice, using periodic boundary conditions. It was formerly shown that the dynamic properties of water and small ions in a single-unit-cell simulation are close to those in a multi-unit-cell simulation [29]. βLG consists of 152 amino acids with 1499 atoms in total. The simulations were done at pH 7. The amino acids GLU and ASP were taken to be deprotonated while LYS, ARG and HIS residues were protonated [30]. This leads to -5 electron charges per protein molecule. Sodium counter-ions were then added for electroneutrality. The crystal structure of βLG was taken from the Brookhaven Protein Database (entry 1B8E [28]) and used as a starting point. Eight protein molecules related by the crystallographic symmetry $C222_1$ were placed in the orthorhombic unit cell with $a = 5.564$ nm, $b = 8.165$ nm and $c = 6.686$ nm. The system consisted of 11992 protein atoms (8βLG molecules per unit cell), 832 crystallographic water molecules (104 per βLG), 3216 added water molecules and 40 sodium ions, leading to a total of 24 176 atoms; figure 1.

2.2. MD calculations

MD simulations were performed in the presence or absence of position restraints on protein atoms, and, for the sake of convenience, are referred to as PR and NPR, respectively. The system was equilibrated for $\tau = 100$ ps using harmonic position restraints (1000 kJ mol^{-1} nm^{-2}). The simple point charge (SPC) model was used to model water [31]. The main advantage is that it can correctly reproduce thermodynamic properties in this mixed (water–protein–sodium) system. In particular, SPC is the better choice in studies of protein–water interfaces over other water models such as SPC/E and TIP; however, its self-diffusivity should be scaled by a constant factor of 1.4 [31, 32]. Simulations used the GROMOS96 force field [33]. In this force field, interactions between atoms are divided into non-bonded interactions, between any pair of atoms that are within a given cut-off radius, and bonded interactions between atoms connected by chemical bonds. In the case of non-bonded interactions (electrostatic and van der Waals), a partial charge and parameters for repulsion and attraction are assigned to each atom. The bonded interaction consists of bond, angle and dihedral terms. A typical effective potential is of the form

$$\begin{aligned} V = & \sum_{\text{bond}} \tfrac{1}{2} k^{\text{b}}_{ij} (r_{ij} - b^0_{ij})^2 \\ & + \sum_{\text{angles}} \tfrac{1}{2} k^{\theta}_{ij} (\theta_{ij} - \theta^0_{ij})^2 \\ & + \sum_{\text{dihedrals}} k^{\Phi} \left\{ 1 + \cos\left[n(\Phi - \Phi^0) \right] \right\} \\ & + \sum_{i<j} \left[\frac{A_{ij}}{r^{12}_{ij}} - \frac{B_{ij}}{r^{6}_{ij}} + \frac{\operatorname{erfc}(\beta r_{ij})}{4\pi\epsilon_0 r_{ij}} q_i q_j \right], \end{aligned} \tag{1}$$

where r_{ij} is the distance between atoms (or united atoms when CH_n groups are treated as one atom) i and j, q_i is the partial charge on atom i, β is a parameter that determines the relative weight of the space sum, erfc is the complementary error function, A_{ij} and B_{ij} are Lennard-Jones parameters, k^{b}, k^{θ} and k^{Φ} are force constants for bonds, angles and dihedrals, n is the dihedral multiplicity and b^0, θ^0, Φ^0 are equilibrium values for the bond lengths, angles and dihedrals. Here, bonds and angles are modelled as harmonic oscillators and the dihedral term is represented by a cosine expansion. The most important assumption is that only pair interactions are taken into account (non-bonded interactions between three or more atoms are

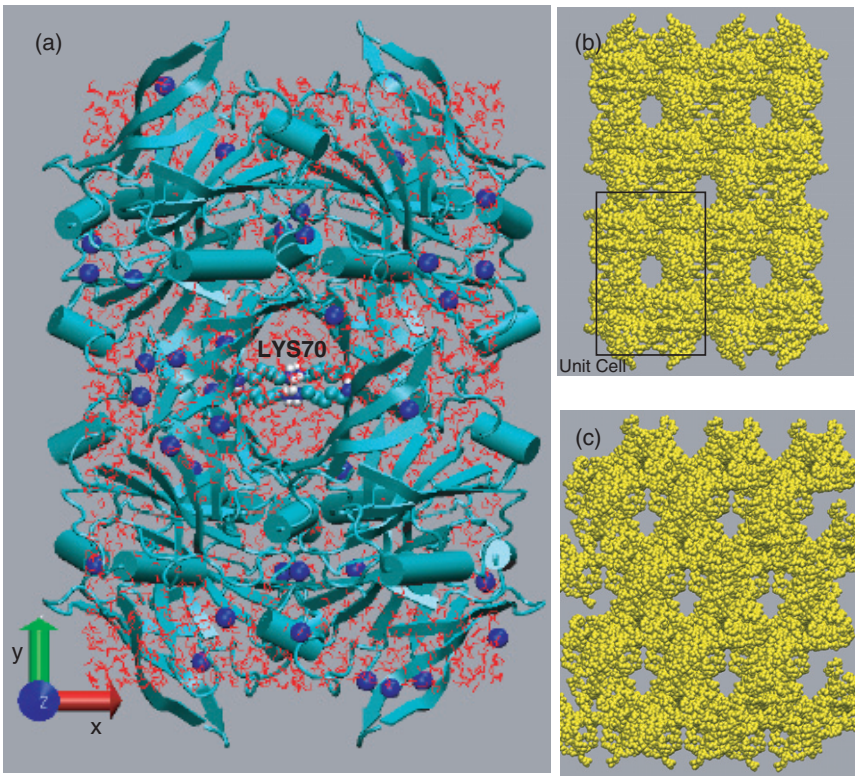

Figure 1. (a) All-atom representation of a single unit cell of an orthorhombic βLG lattice. The view is along the z-axis. LYS 70 residues lie in the pore region. βLG molecules are pictured as cartoons; blue balls represent sodium ions, and water molecules are represented by red lines. The coordinates are: red: X; green: Y; blue: Z. (b) shows the surface representation of a $2 \times 2 \times 2$ βLG lattice along the z-axis. (c) shows the lattice after 45° rotation around the y-axis. The positions of pocket cavities are evident.

neglected). Moreover, atoms are represented as point charges and electronic polarizability is therefore neglected [32]. The long range electrostatic interactions require special care. Lattice sum methods such as Ewald summation or using particle–particle–particle meshes have the disadvantage of enhancing the artefact caused by periodic boundary conditions, which may be of great importance [32–35]. To remove these artefacts associated with truncation of electrostatic forces, electrostatic interactions in our simulations were calculated using the particle mesh Ewald method (PME) with a grid spacing of 0.12 nm and fourth-order interpolation. PME is a method for improving the performance of the reciprocal summation by applying a Fourier transformation on the grid. An inverse transformation and interpolation factors provide the potential and forces on each atom. When Ewald summation is used for long range interactions, the short range Coulomb potential has to be modified. The last term in equation (1) shows the short range electrostatic potential that has been used in our simulation.

MD simulations were performed in a canonical (NVT) ensemble. The temperature was controlled by the Berendsen algorithm, which mimics a weak coupling to an external heat bath at a given temperature T_0. The effect of this weak coupling algorithm is that a deviation of the system temperature from T_0 is slowly corrected according to

$$\frac{\mathrm{d}T}{\mathrm{d}t} = \frac{T_0 - T}{\tau_T}, \tag{2}$$

which means that a temperature deviation decays exponentially with a time constant τ_T. In our simulations, the weak coupling algorithm was applied separately for protein and solvent plus ions with a time constant $\tau_T = 0.1$ ps and a temperature $T_0 = 300$ K. During the simulation, the potential energy and the total energy were monitored in order to check if the system is in equilibrium. Moreover, the profile of the root mean square deviation from the initial configuration was used in order to determine the equilibrium and stability of the protein structure. The cut-off parameters must be comparable to what they were originally assumed to be in the force field. Basically, only the long range cut-off is important for parameterization. For GROMOS96 force fields, the van der Waals cut-off should be $\geqslant$1.4 nm. A cut-off of 1.4 nm was used for van der Waals interactions in our simulations. The integration time step was 2 fs. During the production run, structures were saved every 500 steps (1 ps) and used for analysis. Simulations were done with the GROMACS package [34, 35] (http://www.gromacs.org). Visualization was done by using the VMD v1.8.1 [36] and MOE [37] commercial packages.

3. Results and discussion

Figure 1 shows the instantaneous configuration of the atomic model of a βLG unit cell and its crystal structure. The main pore (PI) in a single unit cell lies along the z-axis. The positively charged LYS70 residues belonging to the βLG molecules in the unit cell lie in the pore space (figure 1(a)).

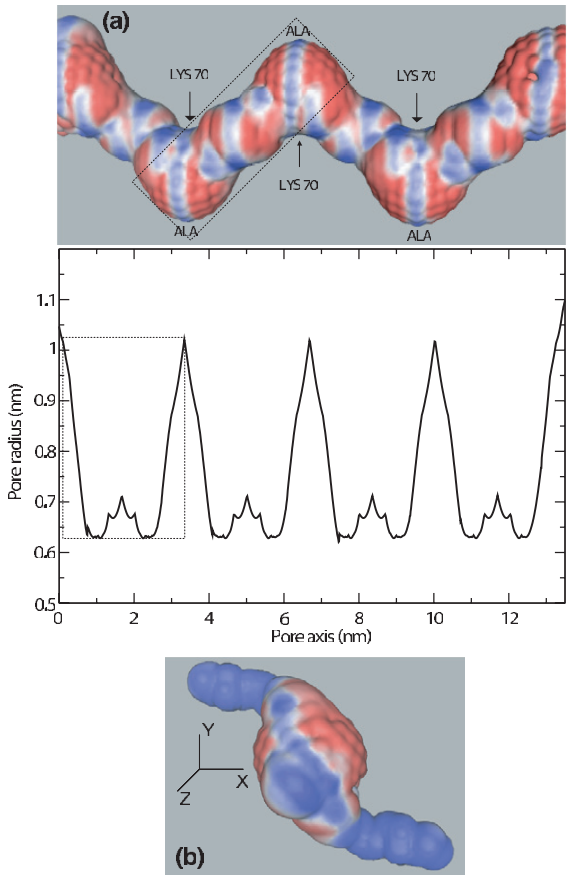

Figure 2. (a) PI pore structure and pore radius profile along the pore axis. Hydrophilic and hydrophobic regions are shown in blue and in red, respectively. The positions of LYS and ALA residues are shown schematically. (b) Shows a pocket cavity in the PII pore.

As we will see, the motion of these residues may affect the pore shape and pore size during the simulation. In each unit cell, there is another pore (PII), perpendicular to the PI pore (figure 1(c)). There are no charged residues lying along the wall of this pore and, therefore, the protein fluctuations do not affect the electrostatic properties of the PII pore. This pore seems more like a series of pocket cavities. Such a pore is not remarkable as a diffusion channel, but could be considered for studying the diffusion anisotropy [11, 14, 16]. Figure 1(b) shows a $2 \times 2 \times 2$ βLG lattice. The positions of the two types of pore are shown in figures 1(b) and (c). In order to determine the pore shape and pore size, the same method as in [16], based on the CHANNEL [38] and HOLE [39] algorithms, is applied here. Figure 2(a) illustrates the pore shape, along with the pore radius profile for PI. PI pores form zigzag channels because of the presence of LYS residues along the z-axis. The position of the LYS and ALA residues is shown in figure 2(a). The profile of the pore size along the pore axis shows that there are constricted zones inside each pore. The pore wall is more hydrophilic in these regions. From the ALA position to a constriction, the pore radius changes from 1.05 to 0.63 nm. The fluctuation of the LYS residues may have a direct effect on the pore size. For PII, on the other hand, the pores can be represented as consisting of big nodes (cavities) with narrow interconnections (figure 2(b)).

The protein fluctuations are summarized in figure 3. Figure 3(a) shows the map of the root mean square displacement of the entire βLG backbone (RMSD), averaged over all eight protein molecules within a 5 ns trajectory. The map represents a matrix, $M(t_1, t_2)$, and was calculated as follows:

$$M(t_1, t_2) = \sqrt{\frac{\sum_i \langle |\Delta \bar{d}_i(\Delta t = t_2 - t_1)|^2 \rangle}{N}}, \qquad (3)$$

where $\langle |\Delta \bar{d}_i|^2 \rangle$ is the average mean square deviation (over all protein molecules) of each backbone atom, i, for each time interval $\Delta t = t_2 - t_1$. $\langle |\Delta \bar{d}_i|^2 \rangle$ is then averaged over all N atoms in the backbone. Each element of the matrix corresponds to a deviation at time $t_2 = t_1 + \Delta t$, compared to an initial time t_1. Figure 3(a) shows that the maximum displacement of the protein backbone as a whole is around 0.265 nm. The light blue region close to the diagonal indicates that there are low relative displacements for small values of Δt. This is due to the restrictions in relative motion imposed by the covalent bonding in the protein structure. Further away from the diagonal, the light blue region corresponds to relatively larger displacements occurring after longer time intervals Δt. The red region with the highest relative displacement appears after the longest time intervals (>2.5 ns). The map also shows that the deviations depend on t_1; therefore, backbone atoms exhibit a time correlated motion.

Figure 3(b) shows the root mean square fluctuation (RMSF) of the C-α of each residue separately for a unit cell of βLG. The fluctuations are consistent with previous works on fluctuations and correlations in the βLG crystal [27, 28]. The RMSF patterns are similar for all eight protein molecules. The residues VAL3, SER36, GLY64, ALA86, PRO113 and PRO126 show fluctuations around 0.125 nm. Among these, GLY64 displays the maximum fluctuations ranging from 0.15 to 0.33 nm. It should be noticed that not all of the residues are accessible from the pore space, as many of them are buried. Indeed, charged residues GLU44, LYS47, GLU55 and LYS70 are directly accessible from the pore space, but, except for LYS70, the rest show fluctuations around 0.05 nm. The pore shape and the pore size are not sensitive to the latter value during a 5 ns MD simulation. For LYS70, however, the fluctuations are more significant, and, consequently, a larger effect on pore shape is expected. The fluctuation for LYS70 ranges from 0.075 to 0.125 nm. Such values can slightly affect the dynamic pore shape. The average pore radius outside the constricted zones is about 0.85 ± 0.05 nm (figure 2(a)). The fluctuation of the corresponding LYS residues may change the pore size up to $(0.075+0.125)/2+0.05 = 0.15$ nm. Moreover, this may change the pore shape to a more cylindrical one, where the residues approach the pore wall. This is shown in figure 3(c) (5 ns).

The water density along the pore axis is an indirect way to look at changes in pore opening during the simulation. The density profile of the water molecules in a pore along the z-axis of the βLG crystal is shown in figure 4. Each unit cell was divided into 25 slices. The number of water molecules in a pore segment within a slice of ~0.2 nm thickness was determined each ps (an intermediate configuration was saved every 500 simulation steps = 1 ps) and was averaged over a 5 ns time

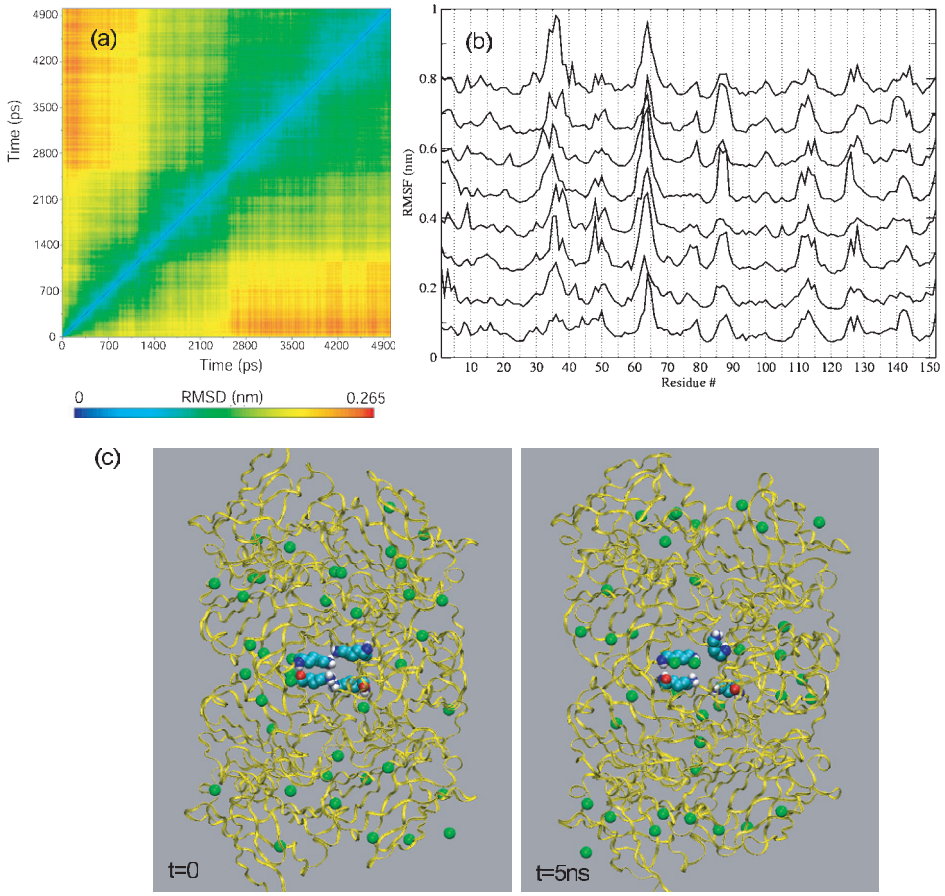

Figure 3. (a) The map of the average backbone root mean square displacement (RMSD) of the βLG protein as a whole over 5 ns. (b) The root mean square fluctuations of the C-α atoms of each residue of each of the eight βLG molecules in a unit cell with respect to its average position. The curves are on the same scale. Each curve is shifted by 0.1 nm in the vertical direction, with respect to the previous one. (c) Displacements of four LYS70 residues inside the pore region are shown by snapshots at the beginning ($t = 0$) and at the end ($t = 5$ ns) of the simulation. Protein molecules are shown as yellow ribbons; green balls represent sodium ions and LYS70 residues are represented by space fills.

interval. Assuming a cylindrical pore segment in each slice and using the pore radius profile (figure 2), the density of water for a given pore segment was calculated by dividing the average number of water molecules by the pore volume of the segment. Mass densities are then calculated from number densities. The density profiles in figure 4 are measured in the absence (NPR) and in the presence (PR) of position restraints on protein atoms. Overall, the density profiles are consistent with the changes in cross-sectional area along the pore axis (see figure 2). The first observation is that the density of water is highest at the pore inlets, where the pores are wider. According to figure 3(c), the pores become locally wider as a result of fluctuations of the LYS70 residues, which leads to a higher water density at those places. In the constricted zones, however, the fluctuation is either small (GLU44, LYS47, GLU55) or perpendicular to the pore surface, so that the density is equal to or more than that in the rigid crystal.

In order to study water motion inside the protein crystal pore space, we take into account that the proteins affect the dynamics of all water molecules. The analysis of water motion in protein crystals is useful, as proteins and other essential biological molecules are in contact via an aqueous medium, and the water content in protein crystals is comparable to that

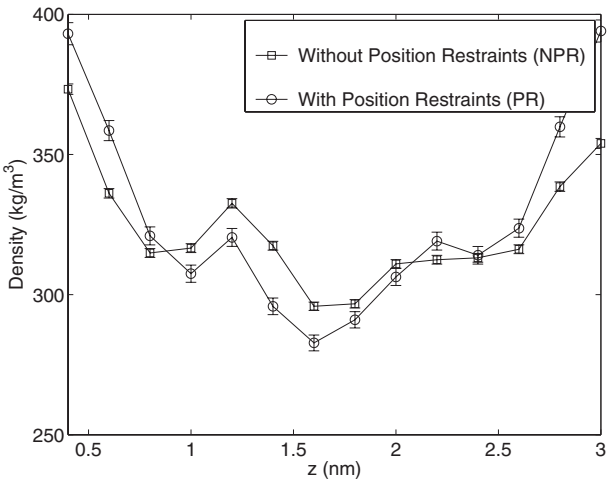

Figure 4. Calculated density (kg m^{-3}) profile of water molecules inside the (PI) pore, along the z-axis.

in living cells [5]. In one of the earliest experimental works on diffusion in protein crystals, Bishop and Richards [6] attempted

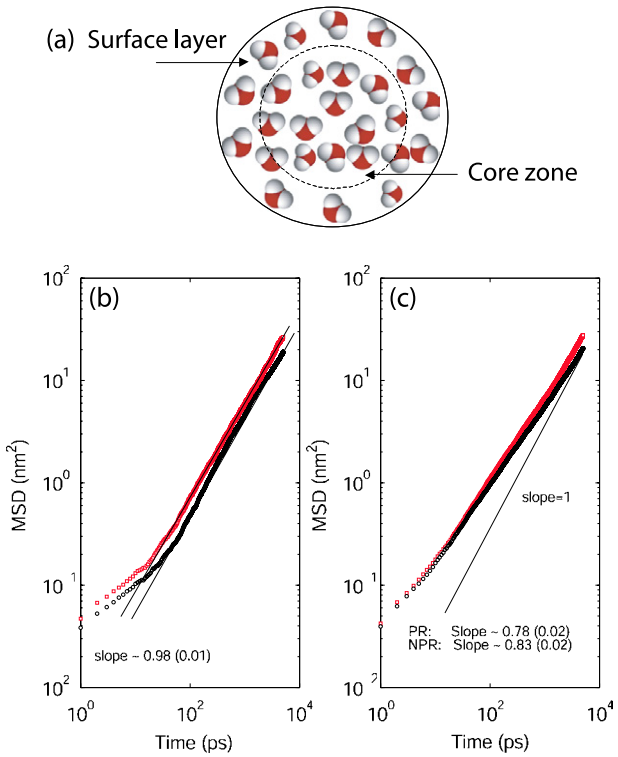

Figure 5. (a) Schematic representation of water molecules in the surface layer and the core zone of a cross-section of a βLG crystal pore. The surface zone corresponds to the first hydration layer, while the core zone corresponds to water molecules further away from the protein surface, in an incomplete hydration layer. (b) Mean square displacement (MSD) of water molecules in the core zone versus time for PR (black) and NPR (red) cases. The value of α in the log–log plot is 0.98 ± 0.01 (95% confidence interval). (c) shows the log–log plot of MSD versus time for the water molecules in the surface layer. The values of α are 0.78 ± 0.02 and 0.83 ± 0.02 for PR and NPR, respectively. The line indicates a trend of $\langle \Delta r^2 \rangle \sim t^1$ (Einstein's law for classical diffusion).

to define the structure of the solvent-containing part of a βLG crystal. Water inside the pore region of a βLG lattice does not exist in a highly ordered form similar to the ice lattice [5, 6, 10]. The pores in a protein crystal have a complicated shape and are not uniform over the length of a unit cell. The treatment of the data in [6] assumed uniform cylindrical pores. The radius of the pores was estimated from the diffusion studies to be between 0.8 and 1.25 nm, close to the pore sizes measured in our study, figure 2(a).

A very recent incoherent quasi-elastic neutron scattering (QENS) experimental study suggested that the water molecules inside a pore region of a triclinic lysozyme crystal could be divided into two populations [12]. The first mainly corresponds to the first hydration layer, and the second to water molecules further away from the protein surface. The diffusion coefficient and transport mechanism are different in those zones. It was proposed that a 'solvent stream' along the protein surface guides the substrate diffusion in the first layer, and led to (quasi-two-dimensional) surface diffusion [12, 40]. Other studies showed an anomalous diffusion behaviour for the water molecules in the first layer [41, 42]. Our recent analysis based on MD simulation of water dynamics in the first layer (surface zone) around the lysozyme molecules in orthorhombic and tetragonal crystals showed that the water molecules in this first hydration layer jump between hydration sites with a broad range of residence times. Such phenomena are expected for the βLG lattice as well. A detailed analysis in terms of protein hydration sites and protein–water interactions is needed to build a precise dynamical model for water molecules in the first hydration layer around βLG molecules. Here, we studied diffusion of water molecules in the surface layer (no further than 0.3 nm away from any protein atoms and no closer than at least 0.1 nm) and in the core zone (at least 0.3 nm away from any protein atom). The definition of these zones is based upon the thickness of a monolayer of water molecules along the protein surface (figure 5(a)). To calculate the water self-diffusion coefficient D in the core, the following relationship is used:

$$D = \lim_{\Delta t \to \infty} \frac{\langle |\Delta \vec{r}|^2 \rangle_{t0}}{6 \Delta t}, \tag{4}$$

where $\langle |\Delta \vec{r}|^2 \rangle_{t0}$ is the mean square displacement (MSD) of water molecules during the time Δt, averaged over the ensemble of water molecules in the core, from the moment t_0 that they entered the core on [41]. In MD simulations, Δt has to be large compared to the correlation time of the velocity autocorrelation function; for the determination of the water diffusivity, this Δt should be at least 20–100 ps [43, 44]. This value may be even higher in the presence of solutes and ions [44]. Moreover, a linear dependence of MSD with time, at large times, has to be verified. Figure 5(b) shows the MSD, calculated for all water molecules in the core zone of the pore at a time interval Δt of 5 ns, in the absence (NPR) and presence (PR) of position restraints on protein atoms. Figure 5(c) shows MSD versus time for water molecules in the surface layer. For the water molecules in the core zone or at very short times (less than 50 ps), the behaviour of the water molecules is not diffusive (MSD is not proportional to t). The curves for $t \geqslant 50$ ps were fitted to a power law expression:

$$\langle |\Delta \vec{r}|^2 \rangle \sim t^{\alpha}. \tag{5}$$

After about 50 ps, the log–log behaviour becomes linear and the slope α becomes very close to one (0.98 ± 0.01). This shows that in a fully hydrated pore of βLG, the water diffusion in the core zone can be described by a Brownian process. Protein atom fluctuations do not affect this behaviour. However, the diffusion coefficients (0.646 ± 0.108 to 0.887 ± 0.41 nm^2 ns^{-1} for PR and NPR, respectively) are slightly different. The diffusion coefficients are less than 17% of the diffusion coefficient, D_0, of free water ($D_0 = 5.2$ nm^2 ns^{-1} at 310 K). This reduction seems to be more significant than could be trivially inferred from purely geometric effects. The fluctuation of LYS70 (obstacle residue) opens the pore and changes the structure of the pore from a zigzag to a quasi-cylindrical channel. This increases the diffusion coefficient of water molecules. The diffusivity values are in good agreement with the experimental values for water diffusion in βLG crystals [6]. Diffusion of water molecules in the layer along the protein surface appears to be anomalous (figure 5(c)). The MSD for water molecules becomes linear after 50 ps. The extracted α values for PR and NPR are 0.78 ± 0.02 and 0.83 ± 0.02, respectively. The slight difference between the

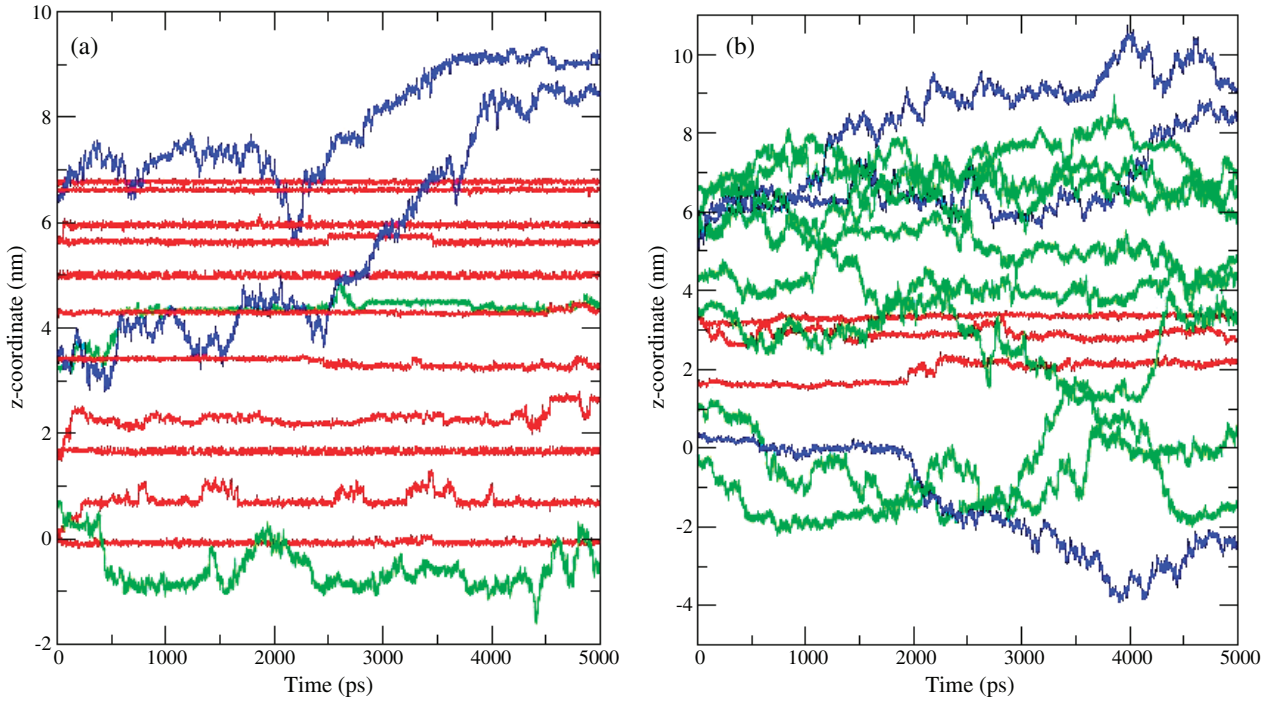

Figure 6. The displacement of a few selected sodium ions along the z-axis through the (PI) pore region for PR (a) and NPR (b) cases. Different colours represent different sodium ions. Blue: ion travels all the way within the pore; green: ion travels partially across the pore; red: the ion remains on the spot with a few motions in x or y directions.

two values might not only occur because of changes in pore size. The strong interactions between the water molecules and hydration sites on the protein surface cause the diffusion to be anomalous. The diffusion behaviour therefore differs from that in the core zone. When water molecules are confined to the proximity of the protein surface, anomalous diffusion can take place [41, 42]. Both the geometrical complexity and the temporal disorder of the water dynamics, i.e., the residence time distribution of water molecules on different protein residues and the protein surface roughness [42], cause anomalous diffusional behaviour. These results show that the motion of water inside the βLG pores is quite different from that of free water. Experimental studies have not been able to reveal this yet [6, 28].

In addition to water molecules, we have also studied the motion of the sodium counter-ions for both PR and NPR simulation set-ups. The motions of the counter-ions around their initial positions were sampled each 10 ps during 5 ns simulations. The location of the ions is sufficiently randomized during the simulation time. Consequently, simulated properties do not depend on the arbitrary initial placement of the ions [20]. Figures 6(a) and (b) show the displacements of 15 out of 40 sodium ions along the z-axis of the unit cell (see figure 1), as a function of time with and without protein restraints. The dynamics of several ions displays jumps, with little motion between jumps. In the case of PR, a few sodium ions travel within the unit cell, although a significant number of ions remain around the same axial (z) coordinate in the pore region, moving rather into the x or y directions. This is not true when protein atoms are flexible (NPR); sodium ions move more freely in this case; some travel all the way within the unit cell, a few remain in the pore and some go deep into the pore and return after some time. It is expected that for longer simulation times, most of the sodium ions will pass the pore. Nevertheless, a 5 ns simulation shows a remarkable difference between the two cases with respect to the effect of protein fluctuations. The presence of positively charged LYS70 residues inside the pore is the main reason for this difference. When the protein is rigid, the LYS residues act as a permanent obstacle for the motion of sodium ions; the pore is very narrow in this case, and there is a strong electrostatic repulsion. The latter accelerates the motion of sodium ions that try to pass through, but prevents complete ion permeation. When there are no position restraints on protein atoms, the positive residues inside the pore move away from the pore space. As a result, there are fewer obstacles, and, consequently, more ions pass through. However, the motion of those ions could be decelerated by the electrostatic interactions with LYS. More analysis at longer times is needed in order to get a better picture of the interactions. We considered all those sodium ions which pass through the pore. The mean square displacement of the ions as a function of time does not show a diffusive motion within the time interval of 5 ns ($\alpha \simeq 0.80 \pm 0.04$). The sodium ions around the charged residues on the protein surface show disordered dynamics, similar to that of the water molecules close to the protein surface (surface zone). Our primary analysis did not show any clear crystal sodium ion sites at the ionic concentration examined ($\sim$0.20 M). Better statistics for the ionic density map may show preferential sites, because the simulation length is still too short to represent the canonical ensemble of sodium ions for our system, since it consists of a rather small number of ions.

Some of the features related to ion transport through ion channels in biomembranes can be obtained by looking at a

protein pore in protein crystals and vice versa [11, 26]. They are made from the same protein constituents; their cross-sections change along the pore axes and their conductivities are comparable. Similarities between ion conduction through protein channels in membranes and protein crystals may clarify the above observations concerning the ion–protein and water–protein interactions during ion and water transport in a non-rigid pore in protein crystals. For instance, it has been shown that in an ion channel, the fluctuations of the protein nanopore from its average configuration would result in a conditional averaged structure. Such an effect in combination with ionic motion inside the protein channel may describe the gating phenomenon [45]. Similar correlations between ionic motion, protein fluctuations and electrostatic interactions exist in a channel of protein crystals. It seems likely that a similar 'gating' effect can describe the acceleration–deceleration of the motion of sodium ions inside a βLG nanopore as well.

4. Conclusions

Molecular dynamics simulations of an orthorhombic βLG lattice were performed for analysing the dynamics of water molecules and sodium ions in the presence or absence of protein fluctuations. Our study suggests that the water molecules inside the pores of a crystal can be divided into a surface layer and a core zone, in agreement with previous QENS studies [12, 24]. The diffusion mechanisms are different in these two zones. Protein fluctuations affect the diffusion constant of the water molecules in the core, increasing the diffusivities from 0.646 ± 0.108 to 0.887 ± 0.41 nm^2 ns^{-1}. The diffusivity of water molecules in the core zone is about 1/6th of the diffusivity of free water. Although water in the core diffuses normally, a continuum diffusion model is still too rough to describe such a confined system (the thickness is about 3–4 water molecules; figure 5(a)). There are both direct and indirect effects of protein–water interactions on water transport, leading to a reduction in diffusivity. Moreover, aspects like the hydrogen-bonding network and dipole–dipole interactions need to be better understood. The values of the pore size (0.63–1.05 nm) and water diffusivities are in good agreement with previous experimental studies [6, 28]. The sodium ions and water molecules close to the protein surface undergo anomalous diffusion. Such anomalous behaviour appears more frequently during transport in disordered, heterogeneous porous media [46].

Although the dynamics of the individual water molecules was not studied in detail, we noticed that many water molecules stayed within their respective zones (core, surface hydration layer), with relatively little exchange between the zones during the time course of the 5 ns simulations. This remarkably slow exchange process is worthy of further computational and experimental investigation.

Acknowledgment

This work was supported by a fund from the LifeTech programme of the Delft University of Technology.

References

[1] Cooper A 2000 *Biophys. Biol. Chem.* **85** 25
[2] Schoenborn B P, Garcia A and Knott R 1995 *Prog. Biophys. Mol. Biol.* **2/3** 105
[3] Ohmine I and Tanaka H 1993 *Chem. Rev.* **93** 2545
[4] Nagendra H G, Sukumar N and Vijayan M 1998 *Protein* **32** 229
[5] Eisenberg D and Kauzmann W 1969 *The Structure and Properties of Water* (London: Clarendon)
[6] Bishop W H and Richards F M 1968 *J. Mol. Biol.* **38** 315
[7] Margolin A L and Navia M A 2001 *Angew. Chem. Int. Edn Engl.* **40** 2204
[8] Vilenchik L Z, Griffith J P, Clair N St, Navia M A and Margolin A L 1998 *J. Am. Chem. Soc.* **120** 4290
[9] Pastinen O, Jokela J, Eerikäinen T, Schwabe T and Leisola M 2000 *Enzyme Microb. Technol.* **26** 550
[10] Granick S 1942 *J. Gen. Physiol.* **25** 471
[11] Morozova T Ya, Kachalova G S, Lanina N F, Evtodienko V U, Botin A S, Shlyapnikova E A and Morozov V N 1996 *Biophys. Chem.* **60** 1
[12] Bon C, Dianoux A J, Ferrand M and Lehmann M S 2002 *Biophys. J.* **83** 1578
[13] Velev O D, Kaler E W and Lenhoff A M 2000 *J. Phys. Chem.* B **104** 9267
[14] Morozov V N, Kachalova G S, Evtodienko V U, Lanina N F and Morozova T Ya 1995 *Eur. Biophys. J.* **24** 93
[15] Cvetkovic A, Straathof A J J, Hanlon D N, van der Zwaag S, Krishna R and van der Wielen L A M 2004 *Biotech. Bioeng.* **86** 389
[16] Malek K, Odijk T and Coppens M-O 2004 *Chem. Phys. Chem.* **5** 1596
[17] Stocker U, Spiegel K and van Gunsteren W F 2000 *J. Biomacromol. NMR* **18** 1
[18] Stocker U, Juchli D and van Gunsteren W F 2003 *Mol. Simul.* **29** 123
[19] Schiffer A C and van Gunsteren W F 1999 *Protein* **36** 501
[20] Walser R, Hunenberger P H and van Gunsteren W F 2001 *Proteins* **43** 509
[21] Palmer A H 1934 *J. Biol. Chem.* **104** 359
[22] Alomirah H, Alli I and Konishi Y 2003 *J. Agric. Food Chem.* **51** 2049
[23] Nishikawa K and Noguchi T 1991 *Methods Enzymol.* **202** 21
[24] Kuroda Y, Hamda D, Tanaka T and Goto Y 1996 *Fold. Des.* **1** 243
[25] Mossolini G E, Lorenzi D, Lioyd D K, McGann A M and Caccialanza G 1998 *J. Chromatogr.* B **712** 83
[26] Tieleman D P, Biggin P C, Smith G R and Sansom M S P 2001 *Q. Rev. Biophys.* **34** 473
[27] Andrade S M, Carvalho T I, Viseu M I and Costa S M B 2004 *Eur. J. Biochem.* **271** 734
[28] Oliveira K M G, Valente-Mesquita V L, Botelho M M, Sawyer L, Ferreira S T and Polikarpov I 2001 *Eur. J. Biochem.* **268** 477
[29] Walser R, Hunenberger P H and van Gunsteren W F 2002 *Proteins* **48** 327
[30] Collini M, Leo B, Baldini G, Monaco H L and Galliano M 2002 *Eur. Bio. J.* **31** 111
[31] Berendsen H J C, Postma J P M, van Gunsteren W F and Hermans J 1981 *Intermolecular Forces* (Dordrecht: Reidel)
[32] van Gunsteren W F and Berendsen J C 1990 *Angew. Chem. Int. Edn Engl.* **29** 992
[33] van Gunsteren W F, Kruger P, Billeter S R, Mark A E, Eising A A, Scott W R P, Huneberger P H and Tironi I G 1996 *The GROMOS96 Manual and User Guide 1996* (Groningen: Biomos and Hochschulverlag AG an der ETH Zürich)
[34] Berendsen H J C, van der Spoel D and van Drunen R 1995 *Comput. Phys. Commun.* **91** 43
[35] Lindahl E, Hess B and van der Spoel D 2001 *J. Mol. Model* **7** 306
[36] Humphrey W, Dalke A and Schulten K 1996 *J. Mol. Graph.* **14** 33

[37] MOE v2002.03 Chemical Computing Group http://www.chemcomp.com
[38] Kisljuk O S, Kachalova G S and Lanina N P 1994 *J. Mol. Graph.* **12** 305
[39] Smart O S, Neduvelil J G, Wang X, Wallace B A and Sansom M S P 1996 *J. Mol. Graph.* **14** 354–60
[40] Bon C, Lehmann M S and Wilkinson C 1999 *Acta Crystallogr.* D **55** 978
[41] Bizzari A R and Cannistraro S 1996 *Phys. Rev.* E **53** R3040
[42] Bizzari A R, Rocchi C and Cannistraro S 1996 *Chem. Phys. Lett.* **263** 559
[43] McQuarrie D A 1976 *Statistical Mechanics* (New York: Harper and Row)
[44] Ahlström P, Teleman O and Jönsson B 1988 *J. Am. Chem. Soc.* **110** 4198
[45] Nadler B, Schuss Z, Singer A and Eisenberg R S 2004 *J. Phys.: Condens. Matter* **16** S2153
[46] Sahimi M 2003 *Heterogeneous Materials I and II* (Heidelberg: Springer)